

Hebron / Ben Nevis rock property analysis and modelling study

Andrew J. Royle, John D. Logel¹, and Laurence R. Lines

ABSTRACT

This paper investigates the sensitivity in amplitude variation with offset (AVO) behaviour with varying rock properties in an attempt to predict oil gravity (density) contrasts. Rock physics scenarios associated with Ben Nevis reservoir zone are performed using Biot-Gassmann fluid replacement modelling to vary porosity, water saturation, and oil density (API). Since, there are numerous variations of these rock properties, AVO modelling volumes are utilized to analyze and interpret the results. Prior to modelling, rock property relationships are observed and used in the AVO modelling analysis. Intercept and gradient volumes were extracted from the data and show variations associated with the rock property models. Crossplots of the intercept and gradient are used to further discriminate the input models. Relationships were observed between the variations in water saturation, porosity, and oil density. Three-parameter AVO techniques are also applied to the volumes in an attempt to predict density variations in the pore fluids.

INTRODUCTION

The Hebron asset is comprised of Hebron, West Ben Nevis, and the Ben Nevis fields. This prospect is located in the southern portion of the Jeanne d'Arc Basin, approximately 350 kilometres from St. John's, Newfoundland (Figure 1). Significant discovery licenses covering this asset were awarded in the mid 1980's based on four exploratory wells over an area of approximately 36 square kilometres.

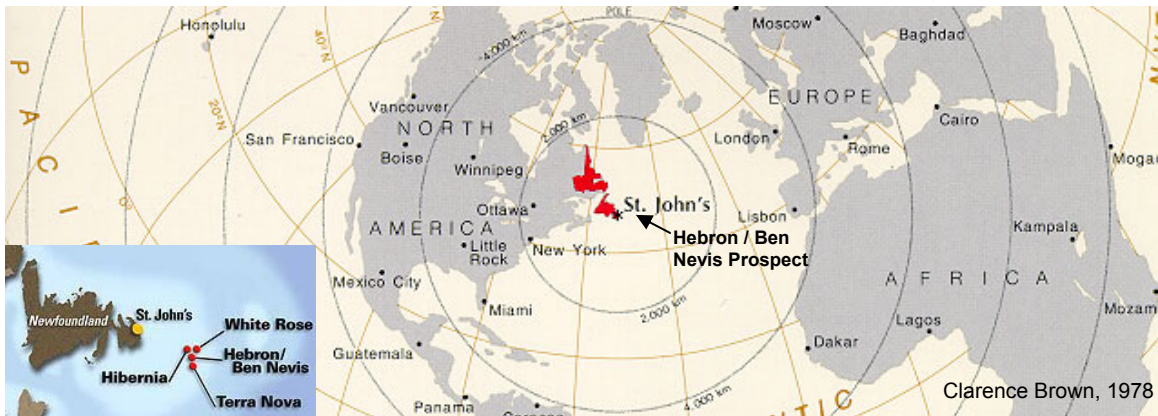


FIG. 1: Hebron / Ben Nevis location map

Oil in place (STOOIP) potential for the asset, including undrilled fault blocks, is estimated to exceed 2 billion barrels. The CNOPB² states that there are 600 million barrels of recoverable oil, based on what has been already drilled (second largest after Hibernia). The upper Ben Nevis horizon encountered significant volumes of “heavy”

¹ Petro-Canada Petroleum Ltd., Calgary, Alberta, Canada.

² Canada-Newfoundland Offshore Petroleum Board

gravity crude in the range of 19- to 21-degree API. Oil is usually classified as heavy if it has API gravities less than 10 degrees (1.0 specific gravity). Therefore, the oil encountered in the Ben Nevis is not as dense as water but still presents production challenges. The thicker oil would require special processing equipment and more than 100 wells might be needed for this development. The Hibernia and Jeanne d'Arc horizons encountered marginal volumes of lighter gravity crude. The Hibernia formation encountered 29-degree gravity oil and the Jeanne d'Arc encountered 30- to 36-degree gravity oil, values similar to that of the Hibernia oil field (Figure 2).

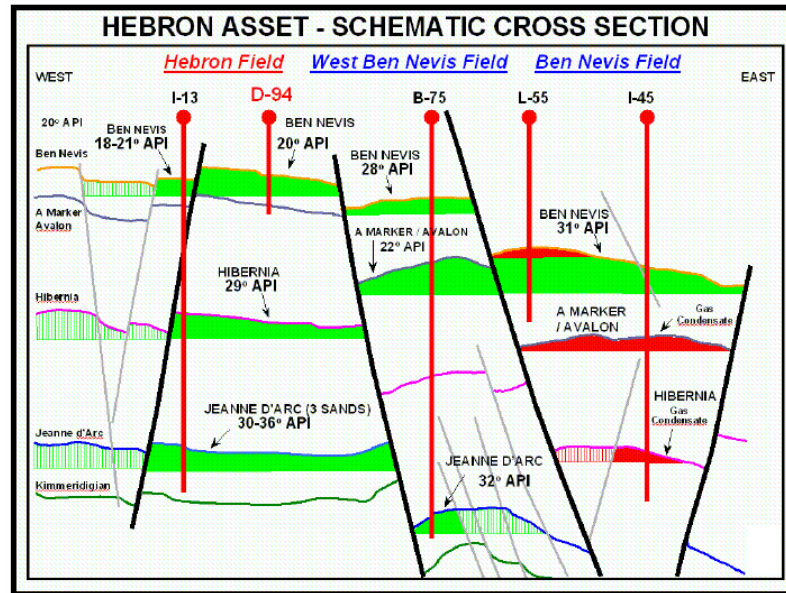


FIG. 2: Schematic cross-section of Hebron /Ben Nevis asset (after Provais, 2000)

AVO as a direct hydrocarbon indicator in clastic rocks is based on changes in the P-wave velocity (V_P), S-wave velocity (V_S), and density (ρ) of a reservoir rock when a hydrocarbon is introduced into pore spaces (Allen & Peddy, 1993). AVO methods have been used successfully to predict hydrocarbons in clastic reservoirs, offshore eastern Canada. AVO is quite useful in the fact that it reduces the drilling risk which is valuable for costly offshore drilling. This method proves to be an excellent exploration tool but traditionally it cannot distinguish between commercial and non-commercial (low hydrocarbon saturation) reservoir zones. This is because the P-wave velocity is very sensitive to the presence of a hydrocarbon in the pore space of a rock even at very low saturation of hydrocarbons. The S-wave velocity and density, however, are not as sensitive to low hydrocarbon saturations in the pore spaces. Using two-parameter AVO equations (e.g., Shuey, 1985, and Smith and Gidlow, 1987) the P-wave velocity is always linked to the shear-wave velocity or density and therefore there is no bias at lower hydrocarbon saturations. Lines (1999), Kelly et al. (2001), Downton (2001), and others have explored a three-parameter AVO extraction in order to get more information from P-wave seismic data in an attempt to isolate rock property contrasts. Kelly et al. (2001) applied this method with good success in the Gulf of Mexico, in an attempt to discriminate between producing and depleted fields.

This method may prove to be an interesting approach at the Hebron / Ben Nevis prospect in an attempt to differentiate between the varying oil gravities. The oil in the Ben Nevis zone has a specific gravity of approximately 0.93, about 0.88 in the Hibernia zone, and approximately 0.84 to 0.88 in the Jeanne d'Arc zone. Therefore, it maybe possible to distinguish between the different gravity hydrocarbons. The Ben Nevis possibly has a gas cap in the structural high regions of the middle fault blocks. This may aid in discriminating some of the reservoir zones and the hydrocarbon boundaries.

In order to get a proper understanding of the rock properties in this region, a rock property study was undertaken to get a better understanding of the reservoir properties. This in conjunction with AVO modelling gives insight into the behaviour of AVO with varying rock properties at the reservoir.

METHODS

Biot-Gassmann fluid replacement modelling (FRM)

The equations for *P*-wave and *S*-wave velocity derived in their most fundamental form using the Lamé coefficients are given by:

$$V_P = \sqrt{\frac{\lambda + 2\mu}{\rho}} = \sqrt{\frac{k + 4/3\mu}{\rho}} \quad V_S = \sqrt{\frac{\mu}{\rho}},$$

where λ is the lamé parameter, lambda; μ is the lamé parameter, mu (shear modulus); k is the bulk modulus, and ρ is the density These velocity equations however, do not take water saturation in to account. These equations are designed to derive velocity of a solid rock (i.e. no porosity). The AVO response is dependent on the properties of P-wave velocity (V_P), S-wave velocity (V_S), and density (ρ) in a porous reservoir rock. This involves the matrix material, the porosity, and the fluids filling the pores. Density effects can be modelled with Wyllie's formula:

$$\rho_{sat} = \rho_m(1 - \phi) + \rho_w S_w \phi + \rho_{hc}(1 - S_w)\phi,$$

where, ρ_{sat} is the density of the saturated rock volume, ρ_m is the density of the rock matrix, ρ_w is the density of water, ρ_{hc} is the density of the hydrocarbon, ϕ is the porosity, and S_w is the water saturation. Independently, Gassmann (1951) and Biot (1956) developed the theory of wave propagation in fluid-saturated rocks, by deriving expressions for the saturated bulk and shear moduli, and substituting into the regular equations for P- and S-wave velocity:

$$V_P = \sqrt{\frac{K_{sat} + \frac{4}{3}\mu_{sat}}{\rho_{sat}}} \quad V_S = \sqrt{\frac{\mu_{sat}}{\rho_{sat}}},$$

where K_{sat} is the saturated bulk modulus, μ_{sat} is the saturated shear modulus, and ρ_{sat} is the saturated density. The ρ_{sat} is derived using the Wyllie's formula that was discussed earlier. In the Biot-Gassmann equations, the shear modulus does not change for varying saturation at constant porosity. Therefore, the shear modulus of the saturated rock (μ_{sat})

equals the shear modulus of the dry rock (μ_{dry}). This is assumed because shear waves should not be affected by pore fluid since they cannot travel through fluids. The Biot-Gassmann bulk modulus equation is given by:

$$K_{sat} = K_{dry} + \frac{(1 - \frac{K_{dry}}{K_m})^2}{\frac{\phi}{K_{fl}} + \frac{1 - \phi}{K_m} - \frac{K_{dry}}{K_m^2}},$$

where, K_{sat} is the bulk modulus of the saturated rock, K_{dry} is the bulk modulus of the dry rock, K_m is the bulk modulus of the matrix, K_{fl} is the bulk modulus of the fluid, ρ is the density. The bulk modulus of the solid rock matrix (K_m) is usually taken from published data that were derived by measurements on core samples. The fluid bulk modulus (K_{fl}) can be modelled using the following equation:

$$\frac{1}{K_{fl}} = \frac{S_w}{K_w} + \frac{1 - S_w}{K_{hc}},$$

where, K_w is the bulk modulus of water and K_{hc} is the bulk modulus of the hydrocarbon. The initial bulk modulus of the dry rock (K_{dry}) can be found by using the following equation:

$$K_{dry} = (1 - y)K_m.$$

Porosity also affects the dry bulk modulus, and this effect can be estimated by using the following equation:

$$\frac{\phi}{K_P} = \frac{1}{K_{dry}} - \frac{1}{K_m},$$

where K_P is the pore bulk modulus (Hampson-Russell Users Manual, 1995). Batzle and Wang (1992) empirical relationships can be used to estimate pore-fluid compressibilities and densities based on reservoir temperature and pressure, oil and gas gravity, gas-to-oil ratio (GOR), and salinity.

AVO methodology

Two-term AVO extraction

Shuey's approximation of the Zoeppritz' equations show the relationship of reflection coefficient versus angle of incidence to changes in impedance and Poisson's ratio. Shuey (1985) approximates the Zoeppritz' equations from Aki and Richards (1980) by eliminating the properties V_S and ΔV_S in the favour of σ and $\Delta\sigma$. Shuey's approximation is as follows:

$$R(\theta) = R_o + \left[A_o R_o + \frac{\Delta\sigma}{(1-\sigma)^2} \right] \sin^2 \theta + \frac{1}{2} \frac{\Delta V_p}{V_p} (\tan^2 \theta - \sin^2 \theta),$$

where R_o is the normal incidence reflection coefficient, A_o is the normal incidence amplitude, σ is Poisson's ratio, $\Delta\sigma$ is the difference in Poisson's ratio ($\sigma_2 - \sigma_1$), and θ is the average angle of incidence measured from the vertical $[(\theta_1 + \theta_2)/2]$. This approximation is commonly used in AVO as it contains three terms separating the normal incidence, small angle (to about 30 degrees), and large angle contributions to the total reflection coefficient at any given angle (Allen & Peddy, 1993). Shuey's approximation gives a relatively simple relationship between rock properties (Poisson's ratio) and the variation in reflection coefficients, and stresses the importance of Poisson's ratio as the primary determinant of the AVO response of a reflection. Shuey's approximation can be simplified even further by omitting the higher order contribution:

$$R(\theta) = R_o + G \sin^2 \theta,$$

where, R_o is the normal incident P-wave reflectivity or "intercept" and G is the "gradient" term. The intercept represents the theoretical zero-offset response; this response will show "bright spots" but does not show any AVO effect. The gradient by definition is the rate of change of the amplitudes at each time sample as a function of incidence angle on a CDP gather. This value should contain entire AVO effect. The intercept and gradient terms from this approximation can be easily obtained through linear regression.

Three-term AVO extraction

In this paper a linearized approach to the Aki-Richards approximation (1980) is used for the three-term analysis. The outputs of the approximation are Intercept (A), Gradient (B), and Curvature (C). The Intercept and Gradient terms should be similar to what is extracted using the two-term extraction. These attribute volumes can be further arranged into P-wave contrast ($\Delta V_p/V_p$), S-wave velocity contrast ($\Delta V_s/V_s$), and density contrast ($\Delta\rho/\rho$) by further manipulation. These volumes give insight on the key rock property contrasts.

In order for accurate results with 3-term AVO approximations, a good angle distribution is needed (~45 degrees), especially for relevant input for the third term.

The Aki and Richards (1980) equation:

$$R(\theta) = A + B \sin^2(\theta) + C \sin^2 \tan^2(\theta),$$

where A , B , and C are defined in terms of the rock property contrasts:

$$A = \frac{1}{2} \frac{\Delta V_P}{V_P} + \frac{1}{2} \frac{\Delta \rho}{\rho};$$

$$B = \frac{1}{2} \frac{\Delta V_P}{V_P} - 2 \left(\frac{V_S}{V_P} \right)^2 \left(2 \frac{\Delta V_S}{V_S} + \frac{\Delta \rho}{\rho} \right);$$

$$C = \frac{1}{2} \frac{\Delta V_P}{V_P}.$$

DATA ANALYSIS

Seven wells have been drilled on the Hebron / Ben Nevis prospect over the last 25 years. In this analysis, wells M-04, D-94, and I-13 are used, all of which encountered pay. There are four key zones of interest: the Ben Nevis formation, the Hibernia formation, and the Jean D’Arc “H” and Jean D’Arc “B” sand reservoirs. The Ben Nevis reservoir is of key interest for this paper due to its low-gravity oil. The goal of this analysis is to detect density differences using a three-parameter AVO extraction in order to obtain a density contrast volumes.

Rock physics analysis

In order to get an understanding of the rock properties associated with the Ben Nevis zone Fluid Replacement Modelling (FRM) was performed on the M-04 well. This well was used because it contained full waveform sonic (*P*-wave and *S*-wave), density, gamma ray, porosity, and other pertinent logs for rock physics analysis. The input logs from the M-04 well are shown in Figure 3. The presence of measured *S*-wave information greatly increases the accuracy of this analysis. This *S*-wave log is of good quality and covers the whole depth of the log suite.

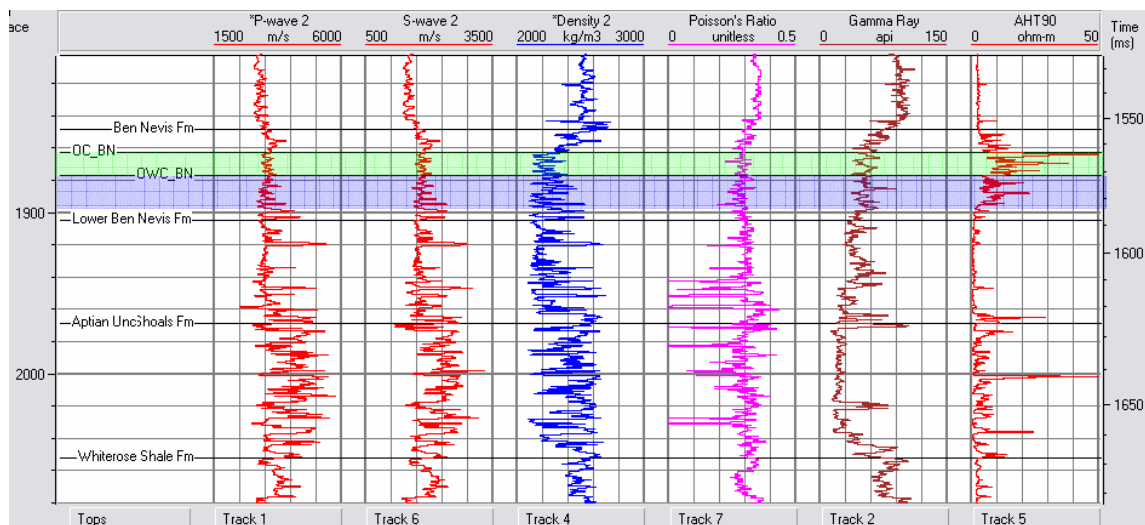


FIG. 3. Original logs at m-04 well location

Prior to FRM the logs were blocked at the key geological boundaries. The input petrophysical for the Batzle-Wang pore-fluid calculations are shown in Table 1. The logs were replaced for perturbations in the oil density (API) and porosity. The API was set

from a range of 16 API to 30 API to simulate realistic variations in the area. The porosity was set to range from 16% to 30% also simulating values found in the general area.

Table 1: Ben Nevis reservoir parameters

Pressure (kPa)	18,800
Temperature (C ⁰)	62
Salinity (Kppm)	60
Oil Gravity (API)	19 - 21 ⁰
Gas/Oil Ratio (m ³ /m ³)	50
Porosity (frac)	0.186 - 0.253
Ave.	0.23
Permeability (md)	320 (10 - 1000)
Water Saturation (frac)	0.35 - 0.20
Ave.	0.246
Oil/ Water Contact (m)	(-1900.7m)
Boi	1.1
Oil Viscosity (cp)	8.0

New P-wave, S-wave, and density logs were output from the Fluid Replacement modelling. Crossplots were made with several different attributes. In Figure 4a the P- and S-wave velocities are crossplotted. Figure 4b shows the crossplot between P-impedance and S-impedance. Figure 4c shows the crossplot between P-impedance and Poisson's ratio. Finally, Figure 4d shows the crossplot between Lambda*Rho and Mu*Rho. The varying porosities are colour-coded and the varying oil density is differentiated by shape. The background points are separated into sandy (gamma ray < 60) and shaley (gamma ray > 60).

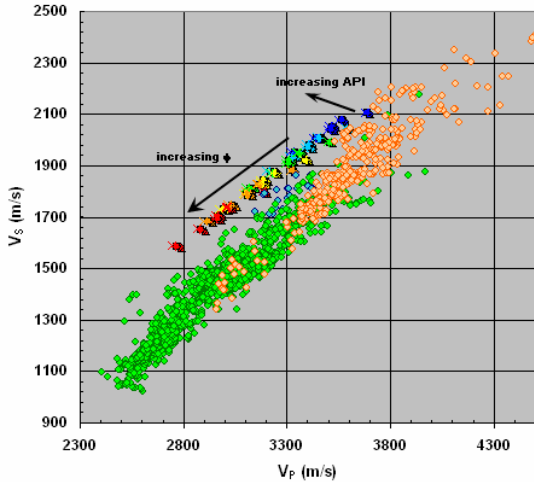
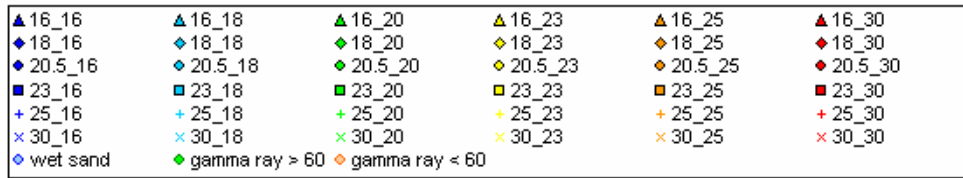


FIG. 4a: V_P versus V_S crossplot

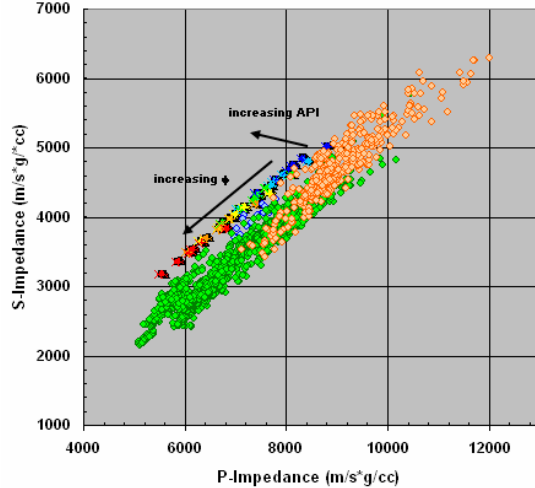


FIG. 4b: I_P versus I_S crossplot

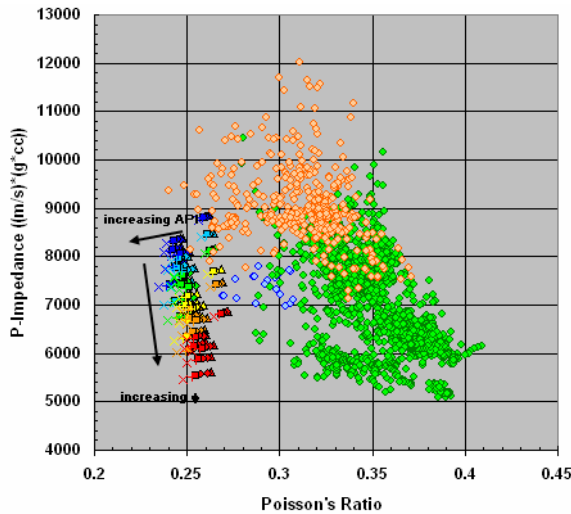


FIG. 4c: Poisson's ratio versus I_P crossplot

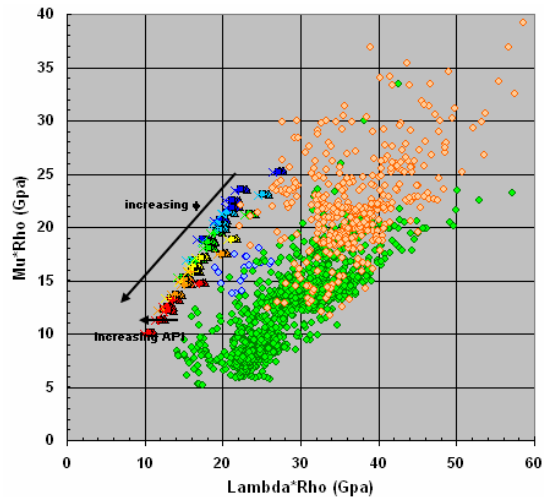


FIG. 4d: $\Lambda \cdot \rho$ versus $\mu \cdot \rho$ crossplot

The crossplots demonstrate that the porosity has a strong deviation between end-members but the changes in API are much more subtle. The API variations, however, are more easily identified on the Poisson's ratio and Lambda-Mu-Rho crossplots than the velocity and impedance crossplots. The porosity and oil density separations seem to be orthogonal to each other on all four plots. The 30% porosity points fall off the background trends much better than the 16% porosity values. The AVO effects are now studied using AVO offset synthetic models.

Synthetic modelling analysis

The AVO modelling volume approach, introduced by Russell et al. (2000), was used to model this data. This approach creates a 3D volume of modelled CDP gathers by varying two physical parameters, one in the inline direction, and one in the cross-line direction (Russell et al., 2000). In our case, three physical parameters were varied, porosity in the in-line direction, water saturation in the cross-line direction, and oil density (API) per volume. A total of six AVO modelling volumes were created for oil densities of 16, 18, 20.5, 23, 25, and 30 API. Once these volumes were attained, regular AVO analysis can be applied to the volumes and interpreted using time slices through the volume. The main focus is on the 20.5 API volume because that is the actual density in the Ben Nevis reservoir in the M-04 well. A cross-line from the 20.5 API modelling volume is shown in Figure 5, the water saturation is 0% and the porosity increases from left to right.

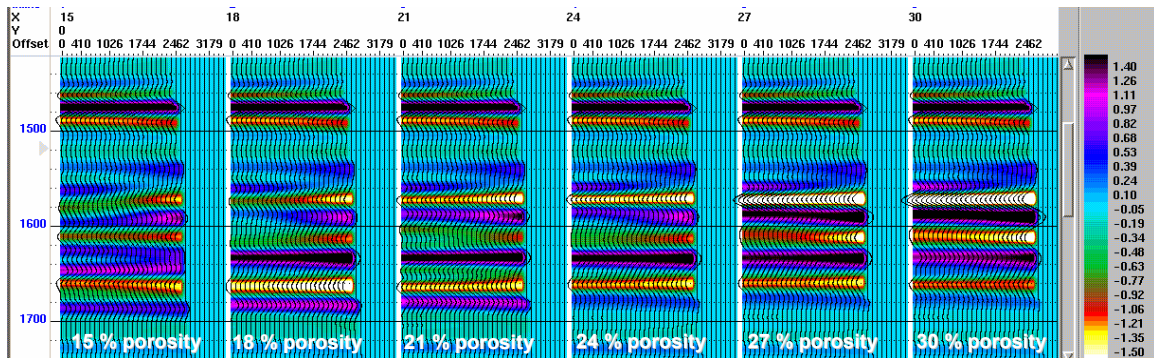


FIG. 5: In-line from 20.5 API modelling volume

The top of the zone of interest is at approximately 1570 ms and the base of the zone (OWC) is at 1590 ms. An AVO anomaly can be seen for the top and bottom of the zone of interest. Porosity seems to have a strong affect on the AVO response. An increase in the amplitude with offset is apparent to about 24% porosity. The amplitude for the top of the zone was picked at 0% S_w and varying porosity for all six volumes and displayed for comparison (Figure 6).

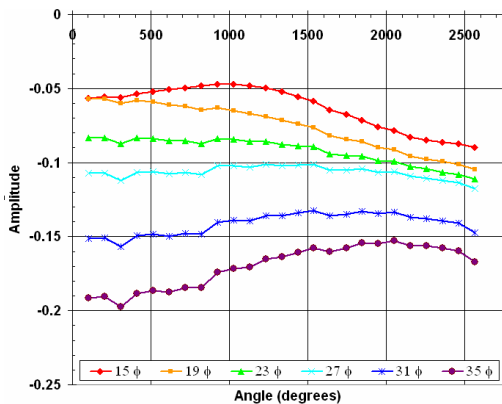


FIG. 6a: Amplitude vs. offset plot for 16 API

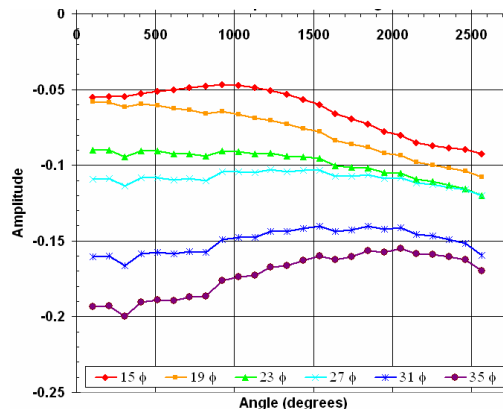


FIG. 6b: Amplitude vs. offset plot for 18 API

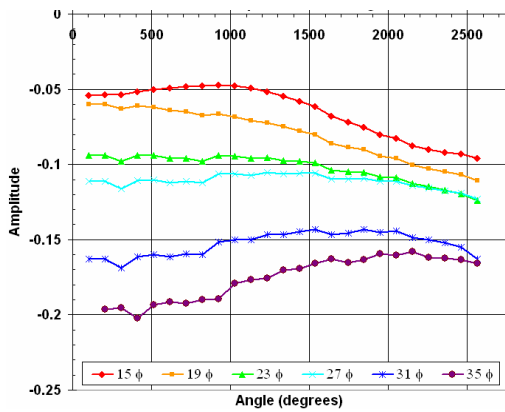


FIG. 6c: Amplitude vs. offset plot for 20.5 API

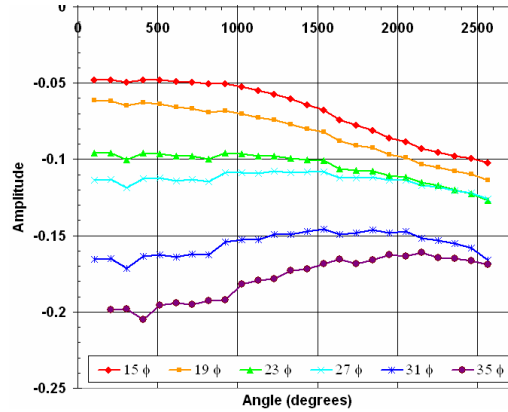


FIG. 6d: Amplitude vs. offset plot for 23 API

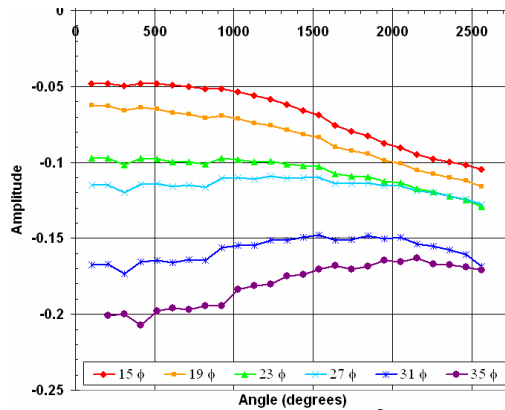


FIG. 6e: Amplitude vs. offset plot for 25 API

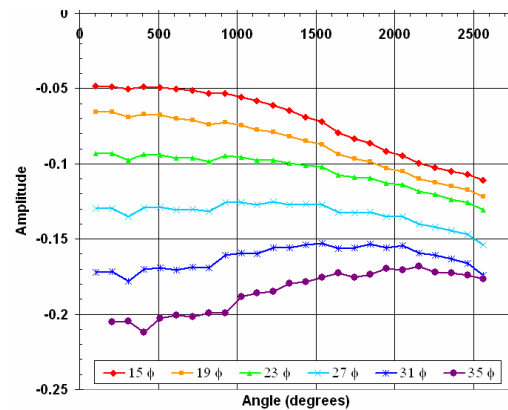


FIG. 6f: Amplitude vs. offset plot for 30 API

It can be seen that the AVO effect at various porosities are stronger with increasing oil density (API) values. This increased AVO effect is quite subtle as seen in the rock physics. It can also be seen that an increase in amplitude with offset (class-3-type AVO anomaly) is present for porosities of 15 to 27% and a decrease in amplitude with offset (class 4 type AVO anomaly) for porosities 31 and 35%.

Prior to the application of the two- and three-term AVO approximations the response of the reflection coefficient with varying offset at the top of the zone of interest was investigated. This is shown in Figure 7 comparing the approximations used in this study.

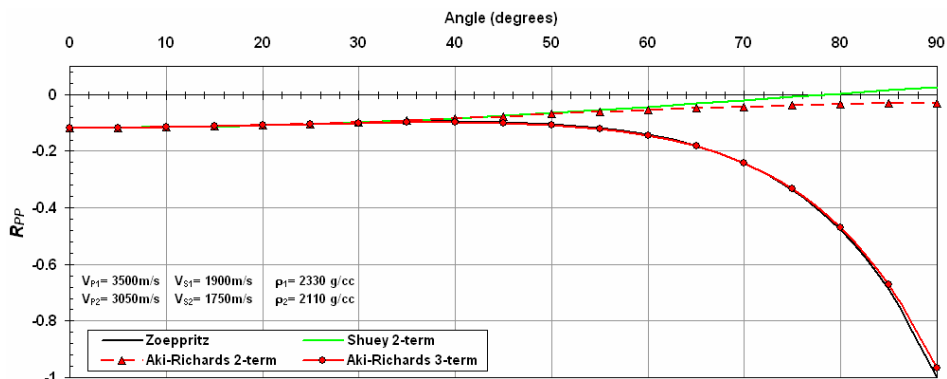


FIG. 7: Comparison of approximations to the exact Zoeppritz at the top of the zone of interest

The black line represents the response of the exact Zoeppritz equations, the approximations are compared to this result for accuracy. The Shuey approximation is accurate to about 32–35 degrees. The Aki-Richards two-term approximation is accurate to about the same as the Shuey. The Aki-Richards three-term approximation almost overlays the exact Zoeppritz to about 80 degrees. It can be said for this study the Shuey (two-term) approximation is good to 32 degrees and the Aki-Richards (three-term) approximation can be theoretically used to 80 degrees. The second term (*B*) of the Aki-Richards contributes to about 32 degrees and the third term (*C*) from 32–80 degrees. These values are taken into account when extracting the AVO attributes.

Intercept (*A*) and gradient (*B*) volumes were created using Shuey's approximation to the Zoeppritz equations. Time slices taken through the top of the zone of interest were created for comparison of the six volumes. This comparison is shown in Figure 8 for the gradient volumes for the top of the Ben Nevis oil zone. The colour bar for these plots is the same so the variation in oil density can be observed. Yellow denotes a strong increase in amplitude with offset, while blue denotes a decrease in amplitude with offset. As seen in the amplitude versus offset plots, porosity has a strong effect on the AVO effect. All volumes show a similar trend with increasing porosity. It can be seen that the AVO effect is strengthening on the 16 API to 23 API volumes at 19–23% porosity. The water saturation seems to have little effect until about 25% on the 15 and 19% porosity in-lines and seems to have no effect when porosity reaches 23%. This may change for even higher water saturations.

Crossplotting of intercept (*A*) and gradient (*B*) data provides useful insight on the nature of the pore fluid. In an intercept versus gradient crossplot brine filled sandstones and shales should fall on a well-defined "background-trend". Outliers from this background trend may possibly indicate accumulations of hydrocarbons or lithologies with anomalous rock properties.

The gradient and intercept volumes are crossplotted to compare the effects of oil density and increasing porosity; this crossplot is shown in Figure 9. Changes in porosity are represented by point colour changes and oil density changes are represented by point shape. On this crossplot, it can be observed that with increasing porosity the anomalous points for the top of the oil zone move from a class 3 type anomaly to a class 4 type anomaly this occurs between 27 and 31 % porosity. The oil density again is less sensitive than the porosity, but separates perpendicular to the background trend. The further away from the background trend the stronger the oil density separation.

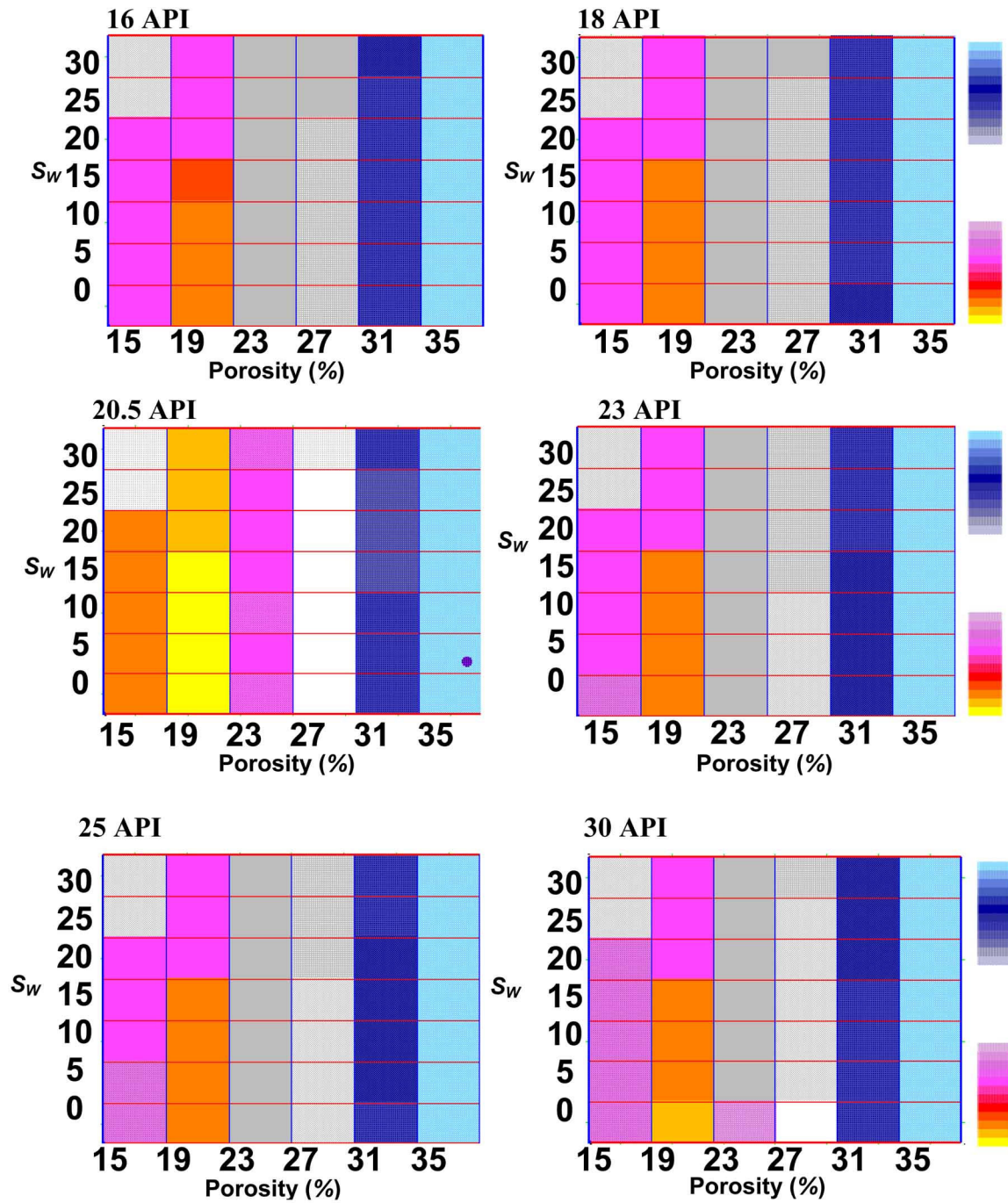


FIG. 8: Time slices for gradient modelling volumes at top of Ben Nevis oil reservoir

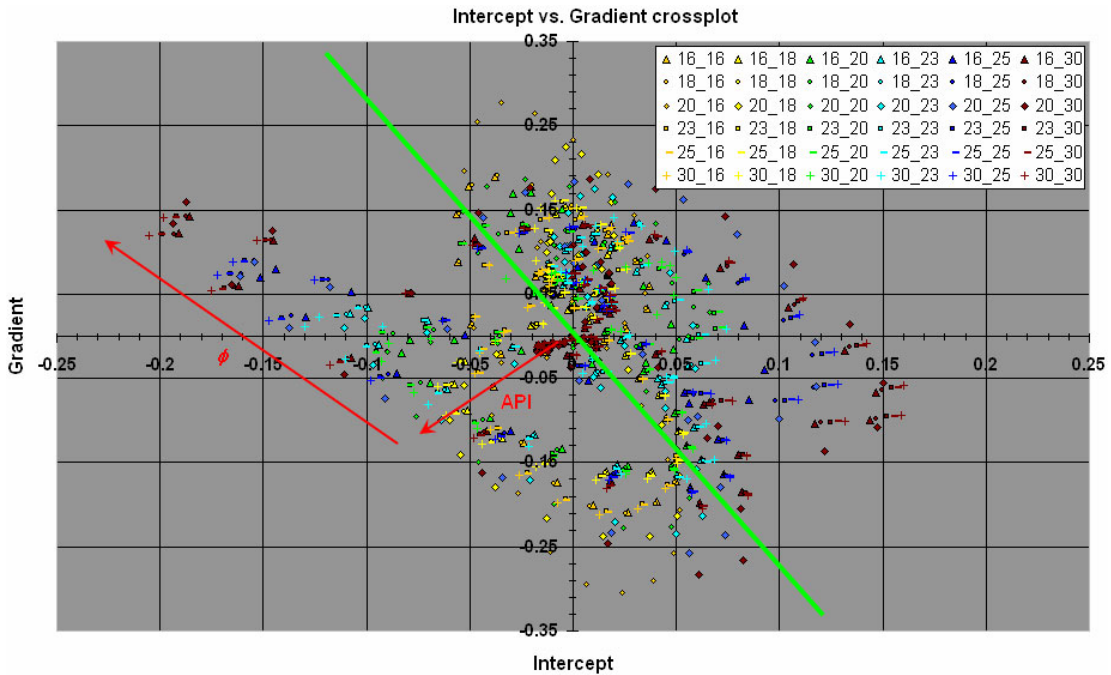


FIG. 9: Intercept versus gradient crossplot for varying porosity and oil density

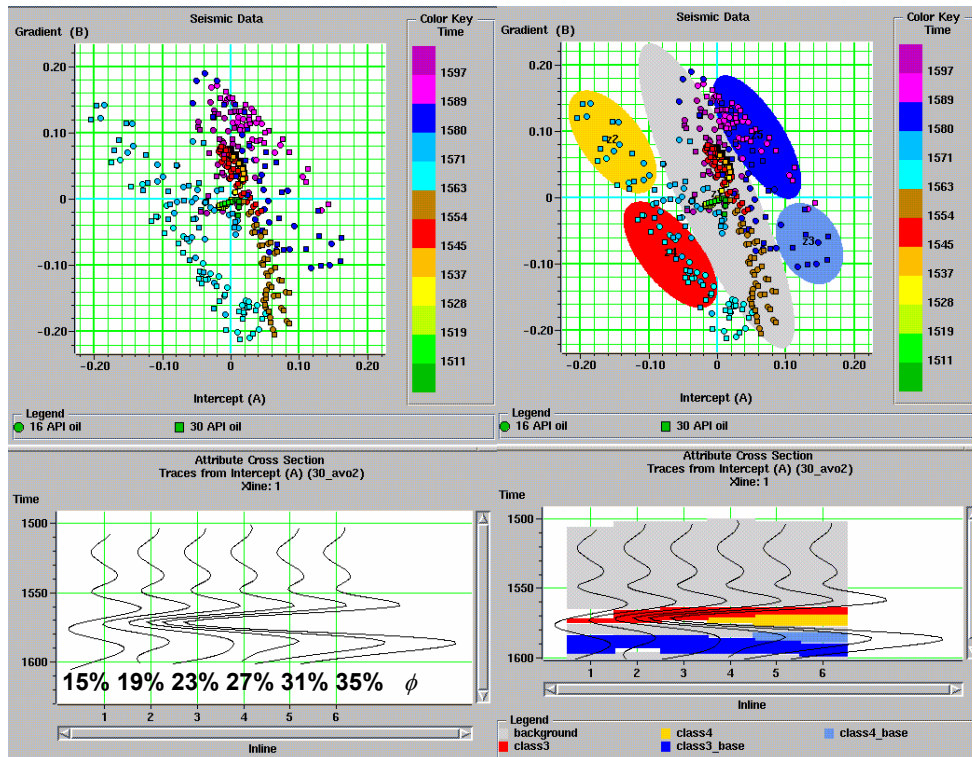


FIG. 10: Intercept versus gradient crossplot for oil densities 16 API and 30 API

Figure 10 shows an intercept versus gradient crossplot for oil densities 16 API (circle) and 30 API (square) with ranging porosities. This shows the background trend (grey), anomalous zones, and their placement on the section. The porosity is increasing from left to right as noted on the section. The highlighted zones on the crossplot are displayed on their respective position on the section below. The strong trough represents the top of the oil zone and the peak below it represents the oil-water contact. The 16-API oil scenario is represented by circles and the 30-API oil scenario is represented by squares. It again is seen on the A-B crossplot, the transition from class 3 to class 4 AVO zones. The 15 % values are almost in the class 2 AVO region. The top of the zone falls off the background trend more than the base (OWC) on the crossplot. This may be because the impedance contrast is stronger for the shale-oil sand interface as compared to the oil sand-wet sand interface.

A three-parameter AVO extraction was utilized in an attempt to detect density variations for the six volumes. Intercept (A), gradient (B), and curvature (C) are the outputs of this extraction. The intercept and gradient terms should be identical to those extracted from the two-term AVO equation. The curvature term only contributes at far offset, so good offset distribution is needed for proper application of three-parameter AVO extractions. Once A , B , and C attributes are acquired, they can be arranged to get P-wave velocity reflectivity ($\Delta V_p/V_p$), S-wave velocity reflectivity ($\Delta V_s/V_s$), and density reflectivity ($\Delta\rho/\rho$). Density reflectivity volumes were created and time slices at the top of the Ben Nevis reservoir are shown in Figure 11.

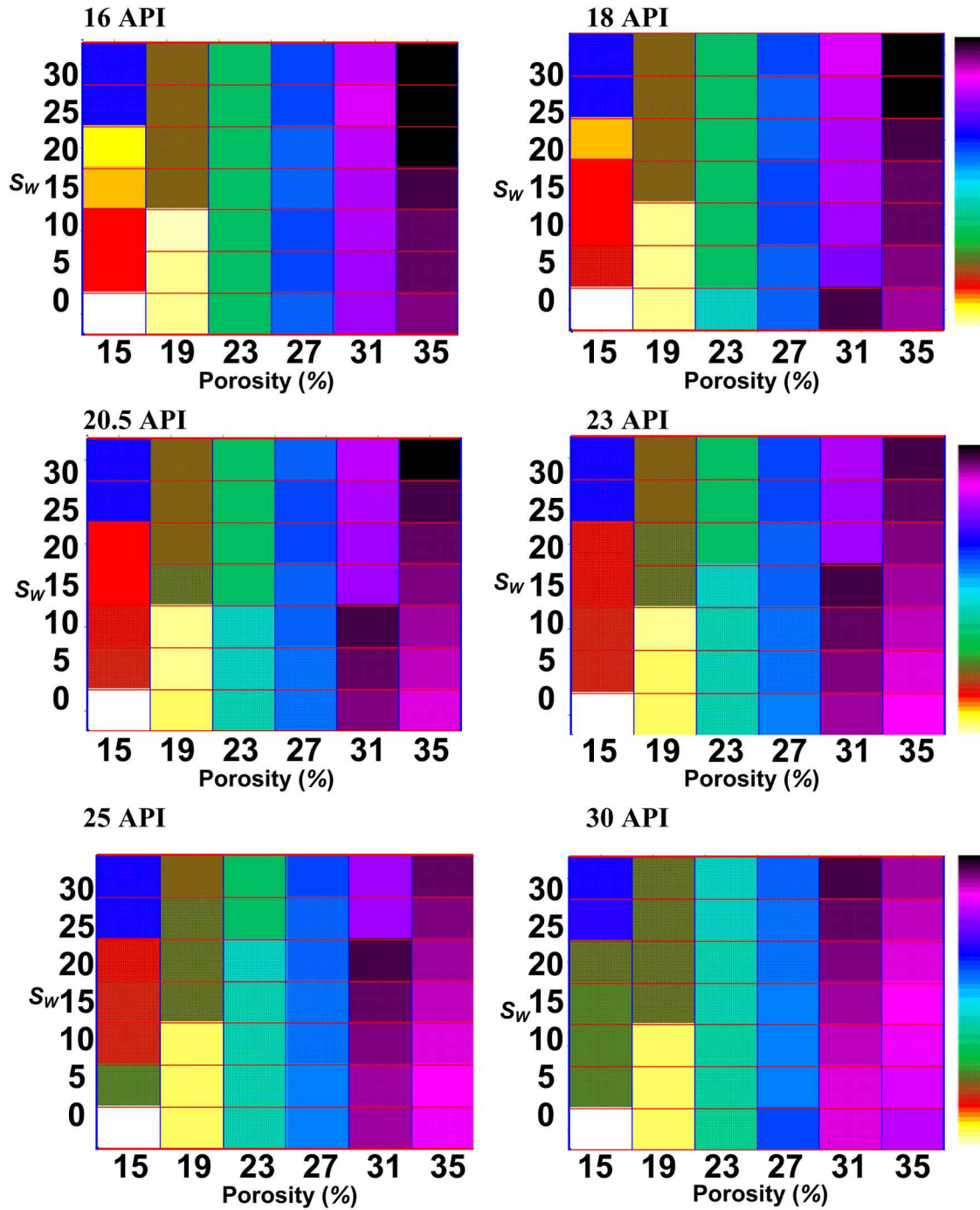


FIG. 11: Density reflectivity time slices at top Ben Nevis zone.

The density reflectivity volumes exhibit variations for the different oil densities. The extreme “darks” represents positive variations and the “hots” represent negative variations. There are strong density contrasts associated with the water saturation within each volumes. There does not seem to be much variation at 15% porosity for varying oil gravity. The variations of density reflectivity with oil density and porosity at 0% water

saturation is shown in Figure 12 and the variations in density reflectivity with oil density and water saturation at 23% porosity is shown in Figure 13.

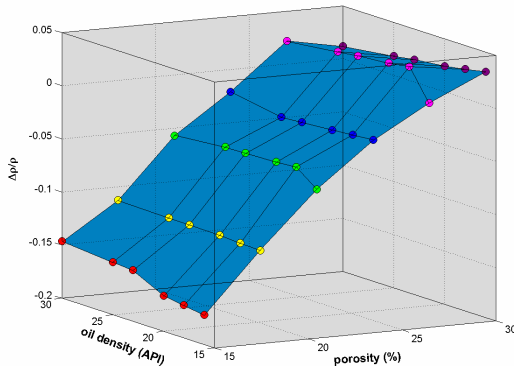


FIG. 12: $\Delta\rho/\rho$ vs. oil density vs. porosity

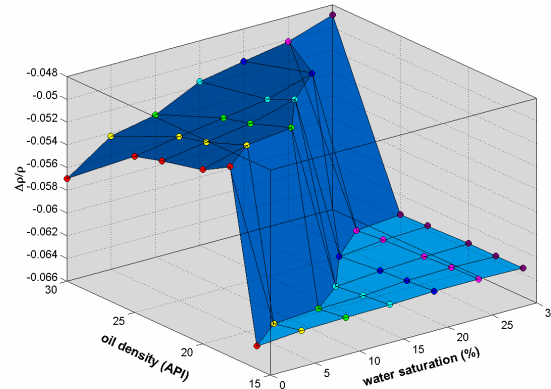


FIG. 13: $\Delta\rho/\rho$ vs. oil density vs. water saturation

Porosity has a strong effect on the density reflectivity values; the oil density also shows variation. The oil density values show stronger negative variations at lower porosities. The water saturation does not have as much effect on the density reflectivity as the porosity. A trend can be seen between the oil saturation and the water saturation. At higher oil densities, the water saturation has less effect on the density reflectivity at lower oil densities the water saturation has more effect on the density reflectivity.

CONCLUSIONS

In this paper, we used Fluid Replacement Modelling to substitute various rock property changes at the Ben Nevis oil reservoir. The rock physics analysis showed the variations at varying porosity and oil density. The oil density and porosity seem to separate perpendicularly for most to the crossplots. The porosity is much more sensitive than the oil density. The points separated quite well on the $\Lambda\rho-\mu\rho$ crossplot compared to the V_P-V_S crossplot.

On the AVO synthetics, the porosity dominated the AVO response dramatically more than the oil density variations. The AVO signature changes from a class 3 type to class 4 type anomaly. The *A-B* crossplots shows the strong effect of porosity, the points for the top of the oil sand move from quadrant 3 (class 3) to quadrant 2 (class 4). The oil density separation with increasing API is stronger further away from the background trend.

The density reflectivity volumes show variations for water saturation, porosity, and oil density variations. The strongest deviations are seen with varying porosity. The oil density shows variations especially at lower porosities. The water saturation shows variation but is not as influential as porosity. A more definitive answer would be attained if two or more wells possibly with different oil gravities in the Ben Nevis reservoir zone are compared.

FUTURE WORK

This study was undertaken to understand the behaviour of the Ben Nevis reservoir zone with varying rock properties as an initial analysis prior to the real data analysis.

Future work would include adding gas and wet cases to the oil sand variations. Also, we wish to incorporate the other two wells in the study area and compare the density contrast values. A test of the uncertainty of three-parameter AVO extractions would also be helpful before proceeding.

ACKNOWLEDGEMENTS

We would like to thank Exxon-Mobil, Petro-Canada, Chevron-Texaco, and Norsk-Hydro for their work on this field and the release of data to the public domain. We would like to acknowledge Gerald Sullivan of Petro-Canada for his help with the geology and petrophysical parameters. We would like to thank Hampson-Russell for the use of their software, especially Brian Russell and Arthur Lee. We also would like to thank the CREWES sponsors for their support of this research.

REFERENCES

- Allen, J.L. and Peddy C.P., 1993, Amplitude Variation with Offset: Gulf Coast Case Studies, SEG, Tulsa, Oklahoma.
- Batzle, M. and Wang, Z., 1992, Seismic properties of pore fluids: *Geophysics*, **57**, 1396-1408.
- Downton, J.E., and Lines, L.R., 2001, Constrained three-parameter AVO inversion and uncertainty analysis, CSEG 2001 Expanded Abstracts.
- Kelly, M., Skidmore, C., and Ford, D., 2001, AVO inversion, part 1: Isolating rock properties: *The Leading Edge*, **20** No. 3, 320-323.
- Kelly, M., Skidmore, C., and Ford, D., 2001, AVO inversion, part 2: Isolating rock properties: *The Leading Edge*, **20** No. 4, 425-428.
- Lines, L.R., 1999, AVO and density: *Canadian Journal of Exploration Geophysics*, **35**, No. 1/2, 32-35.
- Provais, D.A., 2000, Hebron asset Appraisal – East Coast of Canada Case History, GeoCanada Expanded Abstracts.
- Russell, B.H., Lines, L.R., Hirsche, K.W., and Peron, J., 2000, The AVO modelling volume: CREWES Research Report, **12**.
- Shuey, R.T., 1985, A simplification of the Zoeppritz equations: *Geophysics*, **50**, 609-614.
- Smith, G.C. and Gidlow, P.M., 1987, Weighted stacking for rock property estimation in gas sands: *Geophysical Prospecting*, **35**, 993-1014.